2014-08

Local Field Effects for Spherical Quantum Dot Emitters in the Proximity of a Planar Dielectric Interface

UTD AUTHOR(S): Joseph M. Gordon and Yuri N. Gartstein

Gordon, J. M., and Y. N. Gartstein. 2014. "Local field effects for spherical quantum dot emitters in the proximity of a planar dielectric interface." Journal of the Optical Society of America B: Optical Physics 31(9): 2029-2035.

Local field effects for spherical quantum dot emitters in the proximity of a planar dielectric interface

J. M. Gordon and Y. N. Gartstein*

Department of Physics, The University of Texas at Dallas, EC36, Richardson, Texas 75080, USA
**Corresponding author: yuri.gartstein@utdallas.edu*

Received April 11, 2014; revised June 27, 2014; accepted June 27, 2014;
posted June 30, 2014 (Doc. ID 209990); published August 5, 2014

We use numerical solutions of macroscopic Maxwell's equations to study spontaneous emission rates of model spherical quantum dot (QD) emitters in the vicinity of a highly polarizable dielectric substrate. It is demonstrated that extra polarization of the QD body taking place in the interfacial region may lead to appreciable deviations from the rates that would be expected under the assumption of a fixed magnitude of the effective QD transition dipole moment. Illustrations are given for both radiative and nonradiative decay processes, and potential experimental implications are discussed.

OCIS codes: (300.2140) Emission; (160.6000) Semiconductor materials; (250.5590) Quantum-well, -wire and -dot devices; (260.2160) Energy transfer.
http://dx.doi.org/10.1364/JOSAB.31.002029

1. INTRODUCTION

Semiconductor nanocrystal quantum dots (QDs) attract a great deal of attention as versatile light emitters and absorbers for various optoelectronic and biological applications (see numerous references in review articles [1,2]). Their composition- and size-dependent energy gaps allow for easy tuning of the emission wavelength, and the continuing progress in the chemical processing results in high and stable luminescent quantum efficiencies. In one of the recent application targets, colloidal QDs are utilized [3–12] in energy transfer (ET)-based hybrid nanostructures [13] in the role of primary light absorbers to further sensitize adjacent semiconductor substrates/structures for prospective photovoltaic devices. This *excitonic* (by means of ET) sensitization [14] is particularly appealing for crystalline silicon substrates as it would eliminate the weak solar light absorption in the indirect bandgap Si as a defining design factor, thus possibly leading to ultrathin silicon devices. Quantitative experimental studies [7,10,11] of the time-resolved photoluminescence decay revealed that ET from photoexcited QDs into Si substrates can occur by means of both nonradiative (NRET) and radiative (RET) mechanisms exhibiting different distance and wavelength dependencies. These studies demonstrated that QDs on high-refractive-index semiconductor substrates also appear as an interesting practical realization for a general problem of the environmental effects on the emitter's lifetimes [15–17]. It is well recognized now that the spontaneous decay of an excited species depends on the local density of electromagnetic modes, which can be used for purposes of "radiative decay engineering" [15] as well as for engineering of spontaneous emission patterns [18]. Very substantial variations of the QD emission decay rates were, e.g., observed in silicon photonic crystals [19]. Comparisons of decay rates under different conditions serve to evaluate the efficiencies of various decay channels [7,10,15,17].

In this paper, we are concerned with the decay rate of QD excitons in the vicinity of a planar interface, as sketched in Fig. 1, the geometry extensively studied since the original Sommerfeld's treatment [20,21] of the emission by an antenna near the earth's surface. A versatile macroscopic electrodynamics framework has been applied to calculate electromagnetic decay rates and emission patterns for point electric dipole emitters as determined by the polarizabilities of such nonuniform environments (see [16,17,22,23] and multiple references therein). It is known that, for the weak exciton–field coupling, the results obtained in the quantum picture of the exciton decay due to fluctuations of the electromagnetic field are identical to those obtained for classical oscillating dipoles [17]. Experimental studies of the fluorescence decay of atomic/molecular excitons in the vicinity of dielectric and metallic surfaces are well known [16,17,24,25] and compare favorably with the electrodynamics analysis.

Here, we want to assess the specificity of the dielectric polarization effects in the interfacial region with the account of the actual geometric body of the QD. This issue is related to yet another problem with a very long history, that of the local field effects in the theory of dielectrics [26–29]. Discussions of the local field effects on spontaneous luminescence rates of electric dipole emitters embedded in dielectrics have been intensively continuing recently using various microscopic and macroscopic descriptions and treatments of different degrees of sophistication (see, for instance, [29–33] with cited references). The issue of the influence of the uniform dielectric host medium on the emission of QDs has also been addressed theoretically [34,35] and experimentally [36]. The focus of this paper will be on illustrations of the modifications of the luminescence rates owing to the proximity of QDs to the dielectric interface.

In discussing the local field effects due to dielectric polarization in the neighborhood of the excitonic emitter, one wants to distinguish them from the effects due to the spatial extent

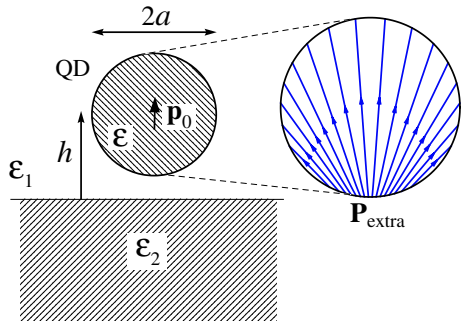

Fig. 1. Sketch of a spherical QD of radius a, with the center at position h from the planar interface between two semispaces of different dielectric constants, ε_1 and ε_2. The QD emitter is represented by the (oscillating) point dipole $\mathbf{p}_0$, embedded at the center of a dielectric sphere of dielectric constant ε. In this example, the dipole is oriented perpendicular to the interface. In the expanded view on the right we show an instance of the extra polarization pattern, $\mathbf{P}_{\text{extra}}$, developed in the QD in the immediate proximity to the interface (see text for details).

of the exciton itself. Given the size of QDs and rapid spatial changes of near fields in (nano) structured environments, considerations of the spatial shape of the excitonic wave functions can be important and may lead to the breakdown of the point electric dipole approximation in the description of the spontaneous exciton decay (see [37,38] and references therein). In particular, substantial wave-function-dependent variations of the decay rates of spatially extended excitons in the vicinity of interfaces were illustrated theoretically [39,40], and the breakdown of the dipole approximation was experimentally shown [37] to be related to the strongly-modified interaction between trapezoidal epitaxial QDs and plasmons in the proximal silver mirror. The analysis in [38] demonstrated that the adequacy of the dipole approximation for the exciton emitter depends on the symmetry of the exciton wave function. Importantly, they proved that, for spherically symmetric wave functions, the size of the wave function does not matter and the point dipole description provides an exact result for the photonic environment effect on the spontaneous emission (Purcell [41] effect). Moreover, this observation turns out to be quite robust with respect to asymmetric deviations from the spherical symmetry [38]. In this paper, we are dealing only with the spherically symmetric emitters and will, therefore, model the excitonic transition in the point dipole description (as sketched in Fig. 1), which makes numerical computations more tractable and local dielectric polarization effects clearly distinguished. It would be interesting to evaluate a possible [38] interplay of the local field and exciton wave function effects in future calculations that explicitly include the spatial distribution of the excitonic transition.

The vacuum spontaneous radiative decay rate of an excited state due to the electric dipole transition with moment $\mathbf{p}_0$ and frequency ω is given by the textbook [17] expression

$$\Gamma_0(\mathbf{p}_0) = \frac{\omega^3 |\mathbf{p}_0|^2}{3\pi\varepsilon_0\hbar c^3}, \tag{1}$$

where c is the vacuum speed of light and ε_0 is the permittivity of free space. Throughout this paper we will be measuring the material dielectric constants in units of ε_0. When the emitter is immersed in the *homogeneous transparent* medium with the dielectric constant ε_{m}, the radiative decay rate becomes equal to

$$\Gamma_{\text{m}}(\mathbf{p}_{\text{m}}) = \sqrt{\varepsilon_{\text{m}}}\,\Gamma_0(\mathbf{p}_{\text{m}}), \tag{2}$$

where the origin of the well-known [17] first factor, the refractive index of the medium, can be readily understood from the structure of expression (1). The influence of local field effects in the uniform dielectric may then be cast in the form of the appearance of the effective (or external [26]) dipole moment $\mathbf{p}_{\text{m}}$. Consider a simple classical model [26] consisting of a dipole with moment $\mathbf{p}_0$ at the center of a dielectric sphere of the dielectric constant ε, which in turn is embedded in the homogeneous medium of the dielectric constant ε_{m}. The standard electrostatic treatments [26,27,42] yield the dipolar field outside the sphere that would be produced by the effective point dipole with moment

$$\mathbf{p}_{\text{m}} = \frac{3\varepsilon_{\text{m}}}{2\varepsilon_{\text{m}} + \varepsilon}\mathbf{p}_0. \tag{3}$$

Expression (3) is valid in the electrodynamics, too, as long as the radius of the sphere is much smaller than the emission wavelength [35]. Given relationship (3), radiative rate (2) is precisely the result derived in the quantum treatment of Ref. [34] for spherical QDs [43]. One notices that with the QD emitter modeled as an oscillating dipole $\mathbf{p}_0$ at the center of a small dielectric sphere, the emission rate in vacuum would be given not by formula (1) but by formulas (2) and (3), with $\varepsilon_{\text{m}} = 1$.

Equation (3) readily illustrates that the magnitude of local field effects on the dipole emission rate can change quite substantially in the interfacial region between two media with different dielectric constants, ε_1 and ε_2, that would lead to two respectively different values of the effective dipole moments $\mathbf{p}_1$ and $\mathbf{p}_2$. In the numerical example studied below, for instance, with $\varepsilon_1 = 1$, $\varepsilon_2 = 16$, and $\varepsilon = 10$, the ratio $|\mathbf{p}_2|^2/|\mathbf{p}_1|^2$ is about 21. In this paper, we will assess the character and spatial extent of these transitional changes via direct solutions of the macroscopic Maxwell's equations using the computational framework provided by the COMSOL Multiphysics software suite [44].

In the context of general discussions of local field effects on guest impurities, the very nature of such direct macroscopic modeling is more in the spirit of the Onsager approach that introduces a real cavity in the host dielectric with a polarizable dipole inside as compared to the Lorentz virtual cavity model [27,29]. Based on calculations with point dipole lattices, it was argued [30] that the virtual cavity model is more appropriate for the emission rates of interstitial impurities while the real cavity model is for substitutional impurities. In our case, indeed, the body of QD is treated so as to substitute the host medium. A distinction, however, needs to be emphasized with the empty cavity model [30,36], since the variable polarization of the QD dielectric material is a very important ingredient in our considerations. At the electrostatic level, the model of QD we exploit in this paper is identical to the model of a molecule used by Fröhlich [26] in the theory of dielectrics. We are not aware of its previous usage for the study of the luminescence decay rates in the interfacial region.

2. COMPUTATIONAL APPROACH AND DETAIL

The electromagnetic decay rate of an oscillating in time, t, electric dipole source, $\mathbf{p}_0(t) = \mathbf{p}_0 \exp(-i\omega t)$, can be conveniently found from the damping reaction (self-) force acting on the dipole [16,17]. Choosing $\mathbf{p}_0$ as a real quantity, it is then the imaginary part of the electric (self) field, $\mathbf{E}$ in the oscillating $\mathbf{E}(t) = \mathbf{E}\exp(-i\omega t)$ at the position of the dipole, that determines the decay rate. The standard classical electrodynamic solution [42] for the electric field of the oscillating dipole in vacuum yields the imaginary part of the field at its position as

$$\mathrm{Im}\,\mathbf{E}_0 = \frac{\omega^3}{6\pi\varepsilon_0 c^3}\mathbf{p}_0. \tag{4}$$

Expression (4) corresponds to the benchmark vacuum decay rate in expression (1). In the quantum language, one could discuss the imaginary part of the self-energy of the excited state with the dipole transition moment $\mathbf{p}_0$. When exposed to various dielectric environments, the electric field $\mathbf{E}$ at the source dipole position also contains the scattered (reflected) field and thereby differs from $\mathbf{E}_0$. Comparing the imaginary parts of the fields, $\mathrm{Im}\,E$ and $\mathrm{Im}\,E_0$, along the dipole direction $\mathbf{p}_0$, would thus determine the resulting decay rate Γ, in terms of the vacuum rate, Γ_0 [16,17]:

$$\frac{\Gamma}{\Gamma_0} = \frac{\mathrm{Im}\,E}{\mathrm{Im}\,E_0}. \tag{5}$$

Relationship (5) is a convenient way of addressing the emission decay rate problem by the numerical solutions of the macroscopic Maxwell's equations yielding the electric field at the position of the same source dipole, $\mathbf{p}_0$, under different conditions.

The setup of the problem we analyze is shown in Fig. 1. The NQD emitter is modeled as an oscillating source dipole $\mathbf{p}_0$ situated at the center of the dielectric sphere of radius a and dielectric constant ε. As we are interested only in the relative changes [expression (5)] of the decay rates as caused by the environment, the very magnitude of the source dipole, $\mathbf{p}_0$, is irrelevant for us here. When needed, it can be evaluated using specific QD exciton models and their wave functions (see, e.g., [34,35,38] and references therein). All of the fields and polarization patterns that we compute would scale proportional to the magnitude of a given $\mathbf{p}_0$. The dielectric sphere itself can assume a variable position with respect to the planar interface between two semispaces of dielectric constants ε_1 and ε_2, respectively. For the display in Fig. 2 we use the convention that position coordinate $h > 0$ is for the center of the sphere in the upper semispace (ε_1), while $h < 0$ means that the source dipole is in the lower semispace (ε_2). The $|h| < a$ positioning corresponds to the sphere crossing the interface boundary.

There are many possibilities for the numerical values of the system parameters. In this paper, we restrict our attention to the values representative of the experiments [6,7,10,11] with CdSe/ZnS colloidal QDs in the proximity to the air–silicon interface. For our examples, we choose the dipole oscillation frequency, ω, corresponding to the vacuum emission wavelength $\lambda_0 = 600$ nm, and the dielectric constants $\varepsilon = 10$ and

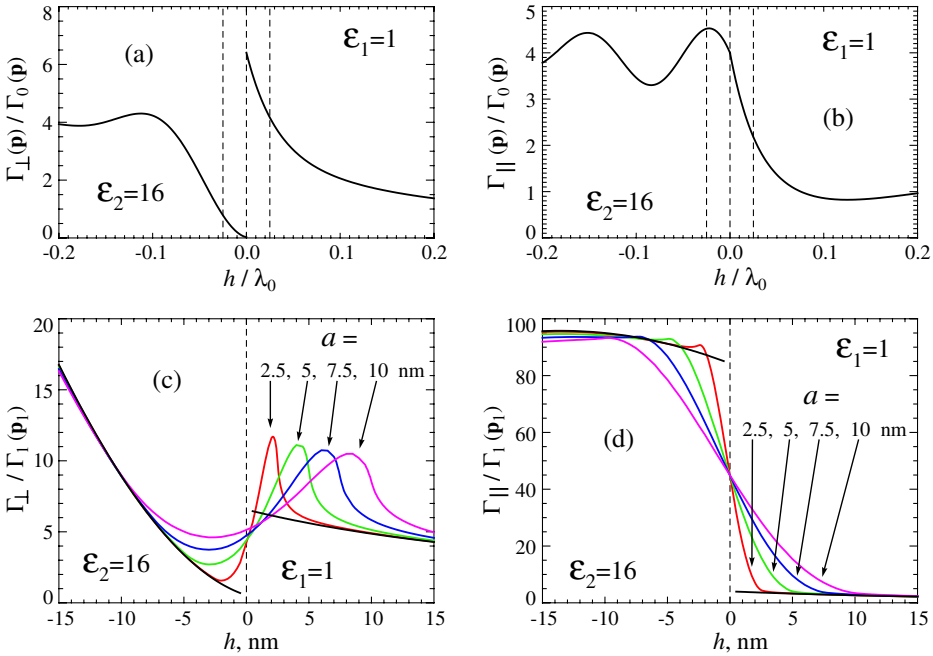

Fig. 2. Radiative emission rates as a function of position h of the emitter with respect to the interface that corresponds to $h = 0$. Panels (a) and (b) show the benchmark variation of the rates in the absence of spatially variable local field effects for two different orientations of the dipole transition moment. The vertical dashed lines define the spatial range of the emitter positions that is displayed in panels (c) and (d), for $\lambda_0 = 600$ nm. The colored lines in panels (c) and (d) show the actual computational results, $\Gamma_\perp$ and $\Gamma_\parallel$, for QDs of different radii a (as indicated) in terms of the emission rate, $\Gamma_1(\mathbf{p}_1)$ in Eq. (2), in the bulk of the semispace with dielectric constant ε_1. The black solid lines show the rates that would be in place for the two fixed effective dipole moments $\mathbf{p}_1$ and $\mathbf{p}_2$ [Eq. (3)], respectively, in the upper and lower semispaces (these correspond to local field effects as they occur far away from the interface).

$\varepsilon_1 = 1$. For illustrations of purely radiative processes, the lower semispace is assigned $\varepsilon_2 = 16$; for illustrations including nonradiative processes, the response of the lower semispace is weakly absorptive with complex-valued $\varepsilon_2 = 16 + i0.3$ (representative of crystalline silicon in this spectral region [45]). The effect of the QD geometric size is demonstrated by comparisons of the results obtained with radius a varying from 2.5 to 10 nm in increments of 2.5 nm.

The computations were performed in the framework of the commercially available COMSOL Multiphysics software package, which is based on the finite elements method. COMSOL has been used extensively, including for modeling involving macroscopic Maxwell's equations [44]. The outer size of the computational domain and intradomain meshing were chosen to balance between the numerical accuracy and computational demands. The outer boundary of the computational domain was assigned an absorbing boundary condition, which simulates an open system. The resulting high fidelity of COMSOL-based computations was verified for the cases where analytical approaches are readily available. That included computations of the self-fields and corresponding emission decay rates [expressions (1) and (2)] in the uniform background spaces as well as the modifications of the decay rates for a fixed value of the effective dipole in the proximity to the interface that are shown in Figs. 2 and 3. The results presented here were obtained with a cylindrical-shaped computational domain of radius $1.25\lambda_0$, and extended to a distance of $1.25\lambda_0$ above and to a distance of 1.5λ below the interface ($\lambda = \lambda_0/4$ being the wavelength in the lower semispace). The inner parts of the computational domain featured two concentric spheres centered around the point source dipole, the smaller sphere of the QD radius and the larger sphere of radius 25 nm for additional control of meshing in the vicinity of the QD upon the approach to the interface.

3. RESULTS AND DISCUSSION

We start with a discussion of purely radiative processes. Our benchmark will be the decay rates due to the electric dipole transition with a fixed value of the effective dipole transition moment. We will refer to such a source as the bare dipole. The effective dipole transition moment for the bare dipole does not depend on the dipole geometrical position with respect to the dielectric environment thereby completely neglecting the role of (variable) local field effects. This is actually the case treated in the macroscopic electrodynamics formalism discussed in [16,17]. Figures 2(a) and 2(b) show the results for the emission rates that are obtained with this formalism as a function of the bare dipole position in the interfacial region. The ratios, $\Gamma(\mathbf{p})/\Gamma_0(\mathbf{p})$, displayed in those figure panels do not depend on the magnitude of $\mathbf{p}$ and are determined exclusively by the reflection properties of the interface [7,10,11,16,17]. The decay rates in the vicinity of the interface depend on the relative dipole orientation, and we show both $\Gamma_\perp$ and $\Gamma_\parallel$ for the dipole oriented, respectively, perpendicular and parallel to the interface. Only far from the interface, at distances longer than the emission wavelengths, would the emission rates stabilize at the bulk values $\Gamma_m(\mathbf{p})$ characteristic

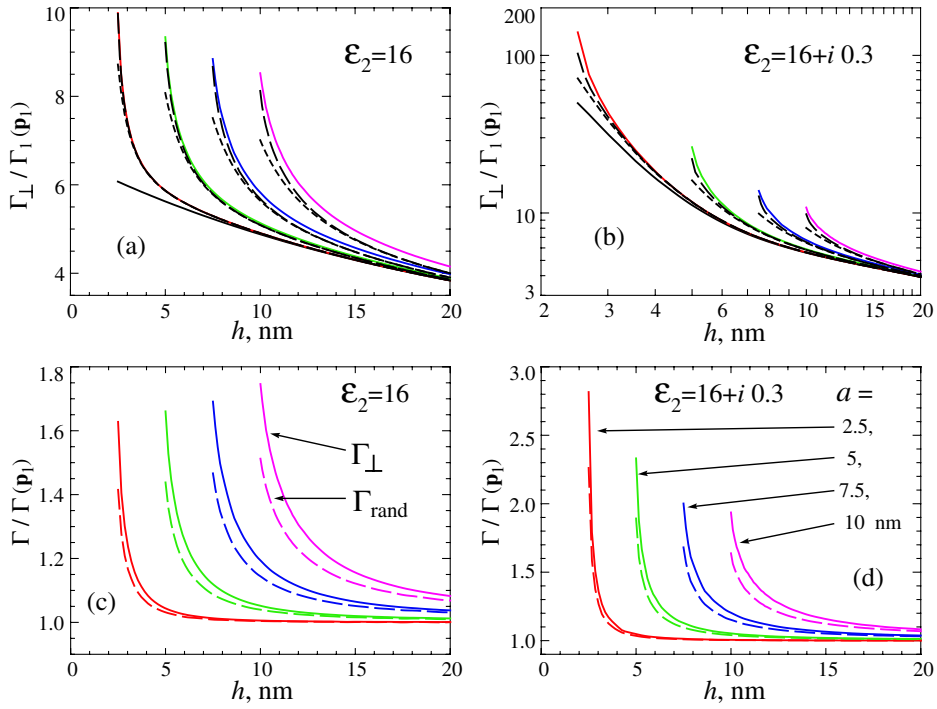

Fig. 3. Emission rates as a function of the QD emitter position $h \geq a$ in the upper semispace with $\varepsilon_1 = 1$ for QDs of different radii a as indicated by coordinated colored lines. The left column, panels (a) and (c), is for a nondissipative substrate with $\varepsilon_2 = 16$. The data in the right column, panels (b) and (d), is for a dissipative substrate with $\varepsilon_2 = 16 + i0.3$. Panels (a) and (b): the colored solid lines show the actual computation results for the model QD emitters with the transition moment perpendicular to the interface in terms of the bulk rate $\Gamma_1(\mathbf{p}_1)$. The solid black lines depict the benchmark results calculated for the fixed bulk value of the effective transition dipole $\mathbf{p}_1$ ("bare dipole"). The black dashed lines are the results that are obtained from benchmarks while taking into account the effect of the extra polarization of the QD body by the substrate in the electric dipole approximation, as derived by using Eq. (6) (short-dashed lines) and by numerically calculating the effective dipole $\mathbf{p}$ (long-dashed lines), see text. Panels (c) and (d) are the ratios of the actual results for model QD emitters and the results obtained for the bare dipoles. The solid colored lines are for the transitions perpendicular to the interface, and the dashed colored lines for the averages over random transition orientations.

of the homogeneous environments, Eq. (2). In the region displayed in Fig. 2, the effects of the interface on the emission rates are evident. As is known [23], the rates exhibit discontinuity at the interface in $\Gamma_\perp(\mathbf{p})/\Gamma_0(\mathbf{p})$ for the perpendicular dipole [panel (a)], but are continuous in $\Gamma_\parallel(\mathbf{p})/\Gamma_0(\mathbf{p})$ for the parallel dipole [panel (b)]. In both cases, however, the rates in the upper semispace with $\varepsilon_1 = 1$ show appreciable growth upon the approach to the interface. This phenomenon is related to the evanescent electromagnetic fields present in the upper semispace and constitutes the basis of the RET mechanism [7,10,11] by which the dipole emission occurs predominantly into the lower semispace with $\varepsilon_2 = 16$.

Should the emission rates of the bare dipole on the different sides of the interface be scaled according to the different fixed values of the effective bulk dipole moments, in expression (3), the interface discontinuities would ensue for both dipole polarizations as shown by the black lines in panels (c) and (d) of Fig. 2 [the ratio $|\mathbf{p}_2|^2/|\mathbf{p}_1|^2 \simeq 21$ is clearly seen in the discontinuity in panel (d)]. That would be reflective of the situation with two fixed but different local fields on the two sides of the interface. In reality, of course, such a scaling is expected to be valid only sufficiently far from the interface, while in its immediate vicinity the local field effects should be variable and dependent on the source dipole position. These expectations are, indeed, what is born out by our computations. The emission rates are found to change continuously as the QD changes its position with respect to the interface; this is shown by the colored lines in Figs. 2(c) and 2(d) depicting the actual results computed with COMSOL for QDs of different radii a. It should be emphasized that the range of QD positions h displayed in panels (c) and (d) is much narrower than the range displayed in panels (a) and (b). It is also clear that the spatial extent of the transitional changes between two semispace scales with the geometrical size a of QDs. This is consistent with the notion that local field effects are basically electrostatic in their origin [27].

The illustrated (generally nonmonotonic) transitional behavior of the radiative emission rates as a function of the QD position would be interesting to access experimentally. That would require, in particular, using QDs with the emission wavelengths in the transparent spectral region of the dielectric surroundings (that is, below the semiconducting bandgap) and building the nanostructures with (partially) buried QDs. The separation of transitions with different polarizations may likely be possible only at low temperatures.

In what follows we address in more detail the question of an immediate practical interest: on the relative importance of local field effects for experiments with QDs in the proximity of silicon-like substrates [10]. For a better perspective on the experimental magnitudes of the decay rates, we note that the photoluminescence decay times, $\tau = 1/\Gamma$, for CdSe/ZnS QDs used in the experiments of [10] on glass surfaces, were measured to be ~20–40 ns in the visible spectral range. These decay times became shorter by factors from ~4 to 7 for QDs on silicon surfaces depending on the wavelength. Figure 3 displays data obtained for model QD emitters with positions $h \geq a$ in the upper semispace, where $h = a$ would signify the QD just touching the substrate. We present the data for both nondissipative ($\varepsilon_2 = 16$) and dissipative ($\varepsilon_2 = 16 + i0.3$) substrates. In the latter case, nonradiative processes can, evidently, very substantially contribute to the overall decay rate of the source dipole within several nanometers from the interface. The nonradiative processes correspond to Joule losses [13,17] due to electrostatic-like near fields of the oscillating dipole. They were clearly distinguished in experiments with colloidal QDs on silicon surfaces [6,7,10,11] and constitute the basis of NRET into the substrate. Once again, the benchmark results are those for the fixed bare dipoles, and they are obtainable with the standard formalism [16,17] and are shown by the black solid lines in panels (a) and (b) of Fig. 3. While converging to the benchmark behavior at larger distances, h, the actual computed data for the model QD emitters [solid colored lines in Figs. 3(a) and 3(b)] evidently exhibit substantial deviations from the benchmarks at shorter distances. To better appreciate the differences, panels (c) and (d) display the ratios of the actual data to the benchmarks. The results in panels (a) and (b) are for the perpendicularly oriented dipoles; the similar in character, but smaller in magnitude, deviations are found for the dipoles parallel to the interface. The ratios in Figs. 3(c) and 3(d) are, correspondingly, also shown for averages over random dipole orientations particularly relevant for experiments with spherical QDs. One observes that QD radius a-dependent trends are different for nondissipative and dissipative substrates. While the benchmark results for NRET (the difference between black solid curves in panels (b) and (a) precisely exhibit a well-known [16,46] $1/h^3$ distance dependence, it is clear from the data shown that the NRET distance dependence for the model QD emitters is steeper.

Simple rationalization of the found deviations can be achieved by recognizing that an extra dielectric polarization of the QD body occurs due to the nearby highly polarizable substrate (thereby specifying "local field effects" in this case). Indeed, consider the following electrostatic "image dipole" [17,27,42] arguments. Start with the original fixed effective dipole $\mathbf{p}_1$ at distance $h > a$ above the interface. The polarization pattern it creates is equivalent to the appearance of its image in the lower semispace. The electric field from the image dipole, in turn, will polarize the dielectric body of the QD. In the simplest approximation of a uniform field $\mathbf{E}_e$ in the medium with ε_1, the additional polarization in the QD corresponds to an additional dipole moment [27]

$$\mathbf{p}_e = \frac{\varepsilon_1(\varepsilon - \varepsilon_1)}{\varepsilon + 2\varepsilon_1} a^3 \mathbf{E}_e.$$

This would, in turn, cause a change in the image dipole, and so on. The self-consistent result in such an approximation is derived by defining the total effective dipole $\mathbf{p} = \mathbf{p}_1 + \mathbf{p}_e$, whose image would produce field $\mathbf{E}_e$ at the position of the geometrical center of QD. The standard electrostatics [27,42] yield

$$\mathbf{E}_e = \frac{2\alpha}{\varepsilon_1 (2h)^3} \frac{\varepsilon_2 - \varepsilon_1}{\varepsilon_2 + \varepsilon_1} \mathbf{p},$$

where factor $\alpha = 1$ for the perpendicular, and $\alpha = 1/2$ for the parallel dipole orientations. Solving for the effective dipole $\mathbf{p}$ would then result in distance h-dependent

$$\mathbf{p}(h) = \mathbf{p}_1 \left[1 - \frac{\alpha}{4} \frac{\varepsilon - \varepsilon_1}{\varepsilon + 2\varepsilon_1} \frac{\varepsilon_2 - \varepsilon_1}{\varepsilon_2 + \varepsilon_1} \left(\frac{a}{h} \right)^3 \right]^{-1}. \quad (6)$$

If one were to apply Eq. (6) to the QD touching the interface, $h = a$, for the highly-polarizable QD body and substrate:

$\varepsilon \gg \varepsilon_1$ and $\varepsilon_2 \gg \varepsilon_1$, then $|\mathbf{p}|^2/|\mathbf{p}_1|^2 \simeq 16/9$ is obtained for the perpendicular orientation, which is quite a noticeable change. The short-dash black lines in panels (a) and (b) of Fig. 3 show the results that one would derive from the benchmark curves due to the renormalization of the effective dipole according to Eq. (6). This renormalization indeed brings the benchmark data closer to the computed colored curves in Fig. 3. It is clear, however, that the picture of a uniform additional polarization of the QD body is not quite accurate at the close approach to the interface. With a nonuniform polarization picture, one would also find that the position of the resulting total effective dipole is somewhat displaced from the geometrical center toward the interface. To further pursue this analysis numerically, we used electrostatic COMSOL calculations to compute actual additional polarization patterns, $\mathbf{P}_{\text{extra}}$, due to the proximity to the interface. Figure 1 displays an example of such a (nonuniform) pattern for the central cross section of the QD with $a = 2.5$ nm just touching the interface. From the computed additional polarization patterns, we calculate (by integration) the additional distance-dependent dipoles $\mathbf{p}_e$ and their center-of-distribution positions. In a manner similar to finding the center-of-mass positions we then evaluate both the resulting total effective dipoles $\mathbf{p}$ (composed of $\mathbf{p}_e$ and $\mathbf{p}_1$) of the QD, as well as their effective positions. The benchmark calculations for the fixed dipole $\mathbf{p}_1$ can now be rescaled with respect to the change of the effective dipole position and its magnitude (a factor of $|\mathbf{p}|^2/|\mathbf{p}_1|^2$). The resulting emission rates for the perpendicular dipoles are shown in panels (a) and (b) of Fig. 3 with the long-dashed black lines. It is transparent that these renormalized results capture the major differences between the original benchmarks and actual electrodynamic COMSOL calculations much better than with the approximation of Eq. (6). Nevertheless, there are still some size- and distance-dependent deviations. Some of them are likely to be related to additional higher-order multipole moments developed in the polarized QD body that cannot be taken into account in the picture of an effective displaced dipole. The example of the polarization pattern in Fig. 1 shows, for instance, that there are components of the quadrupole QD polarization that are parallel to the interface; that is, perpendicular to the original dipole direction in this example. It is worthwhile to stress again that these deviations from the dipolar picture originate from the dielectric polarization in the neighborhood ("local fields") of the original point dipole source $\mathbf{p}_0$. We also note that larger-size QDs can exhibit radius-dependent local field corrections even in the uniform embedding medium [35].

4. CONCLUSIONS

We have used numerical solutions of macroscopic Maxwell's equations to study spontaneous emission rates of model spherical QD emitters in the vicinity of a highly polarizable dielectric substrate. The obtained results illustrate that an extra distance-dependent polarization of the QD body taking place in the interfacial region may lead to appreciable deviations from the rates that would be expected under the assumption of a fixed magnitude of the effective QD transition dipole moment. To a large extent, the deviations can be understood as arising for the electric dipole emitter due to a variable effective dipole moment and a somewhat displaced dipole position.

The spatial extent of the region of appreciable deviations is comparable to the QD size; that is, on the order of several nanometers for ordinary colloidal QDs. We note that this is typically also the spatial scale for significant contributions of nonradiative processes to the QD emission decay. The consideration of the ratio, a/h, of QD radius, a, to distance, h, from its center to the interface affects the practical relevance of the discussed effects for the interpretation of the (available) experimental data. While the largest deviations would be observed for the QD body touching the interface, ligands attached to the QD surface [1] may prevent such positioning. In the experiments of [6,7,10,11] the linking approach was used, where QDs are attached to the silicon surface with chemical linkers of an estimated 1.5–2 nm length. With QDs of radius $a = 2.5$ nm, the numerical data of Fig. 3(d) indicates that the expected deviations at the corresponding distances would likely be too small to distinguish from experimental uncertainties. The situation could be different for shorter linkers and/or larger QDs, as the data in Figs. 3(c) and 3(d) suggests. In this regard, it is important to note studies of so-called "giant" (multishell) QDs that exhibit improved optical properties [47–49]. The increased optical stability of giant QDs make them attractive candidates for ET applications. It would then be interesting to study and analyze ET from such dots in the context of the effects we discussed.

The discussion in this paper has been limited to a specific situation of spherically shaped QDs in the proximity to the dielectric interface. It is understood, however, that similar questions would arise for emitters of other shapes and in the vicinity of other types of substrates, such as metallic structures supporting plasmon excitations. They would require a dedicated quantitative analysis, including the effects "beyond the dipole approximation" for the exciton transition arising from the asymmetric nature of the exciton wave function [38]. This may be a worthwhile undertaking for future studies given the potential opportunities to strongly modify the light-matter interaction in appropriately engineered nanostructures [29,37].

ACKNOWLEDGMENTS

This work was supported by NSF (DMR-1207123) grant. We thank A. V. Malko for many discussions on the subject matter.

REFERENCES AND NOTE

1. D. V. Talapin, J. Lee, M. V. Kovalenko, and E. V. Shevchenko, "Prospects of colloidal nanocrystals for electronic and optoelectronic applications," Chem. Rev. **110**, 389–458 (2010).
2. D. V. Talapin and J. Steckel, "Quantum dot lightemitting devices," MRS Bulletin **38**, 685–691 (2013).
3. S. Lu and A. Madhukar, "Nonradiative resonant excitation transfer from nanocrystal quantum dots to adjacent quantum channels," Nano Lett. **7**, 3443–3451 (2007).
4. S. Chanyawadee, R. T. Harley, M. Henini, D. V. Talapin, and P. G. Lagoudakis, "Photocurrent enhancement in hybrid nanocrystal quantum-dot p-i-n photovoltaic devices," Phys. Rev. Lett. **102**, 077402 (2009).
5. S. Lu, Z. Lingley, T. Asano, D. Harris, T. Barwicz, S. Guha, and A. Madhukar, "Photocurrent induced by nonradiative energy transfer from nanocrystal quantum dots to adjacent silicon nanowire conducting channels: toward a new solar cell paradigm," Nano Lett. **9**, 4548–4552 (2009).
6. H. M. Nguyen, O. Seitz, D. Aureau, A. Sra, N. Nijem, Y. N. Gartstein, Y. J. Chabal, and A. V. Malko, "Spectroscopic evidence for nonradiative energy transfer between colloidal

CdSe/ZnS nanocrystals and functionalized silicon substrates," Appl. Phys. Lett. **98**, 161904 (2011).
7. H. M. Nguyen, O. Seitz, W. Peng, Y. N. Gartstein, Y. J. Chabal, and A. V. Malko, "Efficient radiative and nonradiative energy transfer from proximal CdSe/ZnS nanocrystals into silicon nanomembranes," ACS Nano **6**, 5574–5582 (2012).
8. O. Seitz, L. Caillard, H. M. Nguyen, C. Chiles, Y. J. Chabal, and A. V. Malko, "Optimizing non-radiative energy transfer in hybrid colloidal-nanocrystal/silicon structures by controlled nanopillar architectures for future photovoltaic cells," Appl. Phys. Lett. **100**, 021902 (2012).
9. P. Andreakou, M. Brossard, M. Bernechea, G. Konstantatos, and P. Lagoudakis, "Resonance energy transfer from PbS colloidal quantum dots to bulk silicon: the road to hybrid photovoltaics," Proc. SPIE **8256**, 82561L (2012).
10. M. Nimmo, L. Caillard, W. DeBenedetti, H. M. Nguyen, O. Seitz, Y. N. Gartstein, Y. J. Chabal, and A. V. Malko, "Visible to near infrared sensitization of silicon substrates via energy transfer from proximal nanocrystals: further insights for hybrid photovoltaics," ACS Nano **7**, 3236–3245 (2013).
11. H. M. Nguyen, O. Seitz, Y. N. Gartstein, Y. J. Chabal, and A. V. Malko, "Energy transfer from colloidal nanocrystals into Si substrates studied via photoluminescence photon counts and decay kinetics," J. Opt. Soc. Am. B **30**, 2401–2408 (2013).
12. W. J. I. D. Benedetti, M. T. Nimmo, S. M. Rupich, L. M. Caillard, Y. N. Gartstein, Y. J. Chabal, and A. V. Malko, "Efficient directed energy transfer through size-gradient nanocrystal layers into silicon substrates," Adv. Funct. Mater., doi: 10.1002/adfm.201400667 (2014).
13. V. M. Agranovich, Y. N. Gartstein, and M. Litinskaya, "Hybrid resonant organic-inorganic nanostructures for optoelectronic applications," Chem. Rev. **111**, 5179–5214 (2011).
14. D. L. Dexter, "Two ideas on energy transfer phenomena: ion-pair effects involving the OH stretching mode, and sensitization of photovoltaic cells," J. Lumin. **18/19**, 779–784 (1979).
15. J. R. Lakowicz, *Principles of Fluorescence Spectroscopy* (Springer, 2006).
16. R. R. Chance, A. Prock, and R. Silbey, "Molecular fluorescence and energy transfer near interfaces," in *Advances in Chemical Physics*, S. A. Rice and I. Prigogine, eds. (Wiley, 1978), Vol. **37**, pp. 1–65.
17. L. Novotny and B. Hecht, *Principles of Nano-Optics* (Cambridge University, 2006).
18. L. A. Blanco and F. J. G. de Abajo, "Spontaneous light emission in complex nanostructures," Phys. Rev. B **69**, 205414 (2004).
19. M. D. Leistikow, A. P. Mosk, E. Yeganegi, S. R. Huisman, A. Lagendijk, and W. L. Vos, "Inhibited spontaneous emission of quantum dots observed in a 3D photonic band gap," Phys. Rev. Lett. **107**, 193903 (2011).
20. A. Sommerfeld, "Über die ausbreitung der wellen in der drahtlosen telegraphie," Ann. Phys. Lpz. **81**, 1135–1153 (1926).
21. A. Sommerfeld, *Partial Differential Equations in Physics* (Academic, 1964).
22. L. Luan, P. R. Sievert, and J. B. Ketterson, "Near-field and far-field electric dipole radiation in the vicinity of a planar dielectric half space," New J. Phys. **8**, 264 (2006).
23. C. Creatore and L. C. Andreani, "Quantum theory of spontaneous emission in multilayer dielectric structures," Phys. Rev. A **78**, 063825 (2008).
24. K. H. Drexhage, "Influence of a dielectric interface on fluorescence decay time," J. Lumin. **1–2**, 693–701 (1970).
25. D. H. Waldeck, A. P. Alivisatos, and C. B. Harris, "Nonradiative damping of molecular electronic excited states by metal surfaces," Surf. Sci. **158**, 103–125 (1985).
26. H. Fröhlich, *Theory of Dielectrics* (Clarendon, 1949).
27. C. J. F. Böttcher, *Theory of Electric Polarization* (Elsevier, 1973).
28. V. M. Agranovich and M. D. Galanin, *Electronic Excitation Energy Transfer in Condensed Matter* (Elsevier, 1982).
29. K. Dolgaleva and R. W. Boyd, "Local-field effects in nanostructured photonic materials," Adv. Opt. Photon. **4**, 1–77 (2012).
30. P. de Vries and A. Lagendijk, "Resonant scattering and spontaneous emission in dielectrics: microscopic derivation of local-field effects," Phys. Rev. Lett. **81**, 1381–1384 (1998).
31. P. R. Berman and P. W. Milonni, "Microscopic theory of modified spontaneous emission in a dielectric," Phys. Rev. Lett. **92**, 053601 (2004).
32. M. E. Crenshaw, "Comparison of quantum and classical local field effects on two-level atoms in a dielectric," Phys. Rev. A **78**, 053827 (2008).
33. M. Donaire, "Electromagnetic vacuum of complex media: dipole emission versus light propagation, vacuum energy, and local field factors," Phys. Rev. A **83**, 022502 (2011).
34. A. Thränhardt, C. Ell, G. Khitrova, and H. M. Gibbs, "Relation between dipole moment and radiative lifetime in interface fluctuation qunatum dots," Phys. Rev. B **65**, 035327 (2002).
35. S. V. Goupalov, "Light scattering on exciton resonance in a semiconductor quantum dot: exact solution," Phys. Rev. B **68**, 125311 (2003).
36. S. F. Wuister, C. de Mello Donegá, and A. Meijerink, "Local-field effects on the spontaneous emission rate of CdTe and CdSe quantum dots in dielectric media," J. Chem. Phys. **121**, 4310–4315 (2004).
37. M. L. Andersen, S. Stobbe, A. S. Sørensen, and P. Lodahl, "Strongly modified plasmon-matter interaction with mesoscopic quantum emitters," Nat. Phys. **7**, 215–218 (2011).
38. P. T. Kristensen, J. E. Mortensen, P. Lodahl, and S. Stobbe, "Shell theorem for spontaneous emission," Phys. Rev. B **88**, 205308 (2013).
39. K. J. Ahn and A. Knorr, "Radiative lifetime of quantum confined excitons near interfaces," Phys. Rev. B **68**, 161307 (2003).
40. Y. N. Gartstein and V. M. Agranovich, "Excitons in long molecular chains near the reflecting interface," Phys. Rev. B **76**, 115329 (2007).
41. E. M. Purcell, "Spontaneous emission probabilities at radio frequencies," Phys. Rev. **69**, 37–38 (1946).
42. J. D. Jackson, *Classical Electrodynamics* (Wiley, 1975).
43. Expression (2) refers to the radiative decay rate. If the embedding medium is dissipative, the decay rate can increase substantially due to the absorption in the medium, particularly due to nonradiative energy transfer, and becomes sensitively dependent on radius a of the spherical cavity [28,50]. For small cavities, the NRET contribution that scales $\propto 1/a^3$ can dominate. In the weakly absorbing dielectric, $\varepsilon''_m \ll \varepsilon'_m$, the NRET contribution corresponds to the absorption due to the electrostatic-like field produced by the effective dipole (3), where one could approximately use just the real part, ε'_m, of the dielectric constant.
44. http://www.comsol.com/.
45. D. E. Aspnes and A. A. Studna, "Dielectric functions and optical parameters of Si, Ge, GaP, GaAs, GaSb, InP, InAs, and InSb from 1.5 to 6.0 eV," Phys. Rev. B **27**, 985–1009 (1983).
46. J. M. Gordon and Y. N. Gartstein, "Dielectric polarization, anisotropy and nonradiative energy transfer into nanometer-scale thin semiconducting films," J. Phys. Condens. Matter **25**, 425302 (2013).
47. Y. Chen, J. Vela, H. Htoon, J. L. Casson, D. J. Werder, D. A. Bussian, V. I. Klimov, and J. A. Hollingsworth, "'Giant' multishell CdSe nanocrystal quantum dots with suppressed blinking," J. Am. Chem. Soc **130**, 5026–5027 (2008).
48. H. Htoon, A. V. Malko, D. Bussian, J. Vela, J. A. Hollingsworth, Y. Chen, and V. I. Klimov, "Highly emissive multiexcitons in steady-state photoluminescence of individual giant CdSe/CdS core/shell nanocrystals," Nano Lett. **10**, 2401–2407 (2010).
49. A. V. Malko, Y.-S. Park, S. Sampat, J. Vela, Y. Chen, J. A. Hollingsworth, V. I. Klimov, and H. Htoon, "Pump-intensity- and shell-thickness-dependent evolution of photoluminescence blinking in individual core/shell CdSe/CdS nanocrystals," Nano Lett. **11**, 5213–5218 (2011).
50. S. Scheel, L. Knöll, and D. G. Welsch, "Spontaneous decay of an excited atom in an absorbing dielectric," Phys. Rev. A **60**, 4094–4104 (1999).